# Head Loss Analysis on Acoustic Propagation on Duct Discontinuities of H-Type Microcells

**R. Yosi Aprian SARI** *
*Physics Education Department, Faculty of Mathematics and Natural Sciences, Universitas Negeri Yogyakarta, Jl. Colombo No. 1, Karangmalang, Yogyakarta, 55281, Indonesia, ryosia@uny.ac.id*

**Restu WIDIATMONO**
*Physics Education Department, Faculty of Mathematics and Natural Sciences, Universitas Negeri Yogyakarta, Jl. Colombo No. 1, Karangmalang, Yogyakarta, 55281, Indonesia, restu@uny.ac.id*

**Rida Siti Nur'aini MAHMUDAH**
*Physics Education Department, Faculty of Mathematics and Natural Sciences, Universitas Negeri Yogyakarta, Jl. Colombo No. 1, Karangmalang, Yogyakarta, 55281, Indonesia, rida@uny.ac.id*

**Kuncoro Asih NUGROHO**
*Physics Education Department, Faculty of Mathematics and Natural Sciences, Universitas Negeri Yogyakarta, Jl. Colombo No. 1, Karangmalang, Yogyakarta, 55281, Indonesia, kuncoronugroho@uny.ac.id*

* Author to whom correspondence should be addressed

*Abstract:* - A sudden change in the duct's cross-sectional area significantly impacts the head loss-causing acoustic propagation pressure. This article discusses how the optimal design of the H-type microcells is affected by head loss as a function of the duct cross-sectional area. The impedance limit requirements are taken into account when optimizing the microcell design. Transmission Matrix Method (TMM) and Genetic Algorithm (GA) optimization techniques are utilized to examine the duct's acoustic propagation and the duct's cross-sectional area change. The results obtained from this optimization are: buffer length in the range 48.75 mm – 48.83 mm, buffer radius in the range 8.78 mm – 8.79 mm, microcell length in the range 107.46 mm – 107.47 mm, and a microcell radius of 2.93 mm, with a resonance frequency in the range 1543.73 Hz – 1543.93 Hz.

*Keywords:* - optimal design of the H-type microcells, head loss, impedance, transmission matrix method, genetic algorithm.

## 1. INTRODUCTION

Wave propagation is simple when the propagation plane is uniform, but the issue becomes more challenging when there is a duct discontinuity. A duct discontinuity is an abrupt change from a large to a small cross-sectional area (contraction) or vice versa (expansion). This duct discontinuity application is widespread, even in the realm of bioengineering. For instance, a sudden network of blood vessels contracting is seen as a pipe flow.

Edge effect singularities are several effects from this duct discontinuity, such as variations in pressure in each plane and changes in the locations of the pressure peaks. It is crucial to optimize the duct geometry to increase the pressure, which is often low. Due to its straightforward symmetry, which matches the direction of wave propagation along the cylinder's axis or one of its axes, the cylindrical duct arrangement is the one that is most usually utilized in this situation.

Miles [1], [2] was the first to study duct discontinuities. He formulated the fundamental equations for wave propagation near the discontinuities and demonstrated that the duct discontinuities can be compared to impedances. Following this, Karal [3] looked into the acoustic inductance for line discontinuities in two circular ducts of infinite length and various cross-sections that work together to form an acoustic transmission system. Here, he adds that the acoustic pressure that travels through the micro-cell (a duct with a smaller

radius) only holds at extremely low frequencies.

Simulation or modeling can obtain the necessary predictions with some accuracy. This problem's modeling development relates to sonic propagation in three cylindrical tubes joined together on one axis to produce a system known as a microcell. In the field of photoacoustics, Tavakoli et al. [4] employed an electrical transmission model that resembles a microcell, Cai et al. [5] used the four-pole network method, and Duggen [6] used FEM to simulate photoacoustic signals in cylindrical micro-cell photoacoustic cells. The experiment by Rey et al. [7] was designed to produce the strongest photoacoustic signal. The length of two cylinders with a high cross-sectional area flanking a tiny cylinder cross-sectional area was also the subject of research by Rey and Sigrist [8]. Another finding by Mannoor et al. [9] measured the performance of cells with different dimensions using statistical and parametric analyses.

## 2. ACOUSTIC PROPAGATION IN H-TYPE MICROCELLS

Acoustic propagation produces convection waveforms. The convection wave equation in the z-direction is [3], [10], [11]:

$$\begin{aligned} &\nabla^2 p(\vec{r},\omega) + k_0^2 p(\vec{r},\omega) = 0 \\ &\partial p/\partial n = 0 \quad \text{on} \quad \Gamma_1 \cup \Gamma_2 \cup \Gamma_3 \cup \Gamma_4 \cup \Gamma_5 \end{aligned} \tag{1}$$

where $k = \omega/c_s$ is the wave number, $\omega$ is frequency and $c_s$ is the speed of sound. *A*, *B*, and *C* cylinders are coupled to each other so that the azimuth normal mode form must be orthogonal and axis-symmetric, i.e. $m = 0$ (see Figure 1).

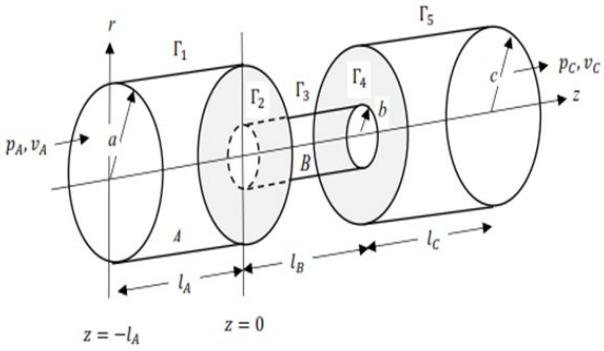


**Figure 1**. H-type microcells system

The general solution of equation (1) relating to the three coupled cylinders is Liu *et al.* [12]:

$$p(r,z) = \begin{cases} \sum_{n=0}^{\infty} \left\{ \begin{matrix} \left[A_n^+ e^{ik_{zA}(z+l_A)} + A_n^- e^{-ik_{zA}(z+l_A)}\right] \\ \times J_0\left(\frac{\pi\alpha_{0n}}{a} r\right) \end{matrix} \right\}, \begin{cases} -l_A \le z \le 0 \\ 0 \le r \le a \end{cases} \\ \sum_{n'=0}^{\infty} \left\{ \begin{matrix} \left[B_{n'}^+ e^{ik_{zB}z} + B_{n'}^- e^{-ik_{zB}z}\right] \\ \times J_0\left(\frac{\pi\alpha_{0n'}}{b} r\right) \end{matrix} \right\}, \begin{cases} 0 \le z \le l_B \\ 0 \le r \le b \end{cases} \\ \sum_{n''=0}^{\infty} \left\{ \begin{matrix} \left[C_{n''}^+ e^{ik_{zC}(z-l_B)} + C_{n''}^- e^{-ik_{zC}(z-l_B)}\right] \\ \times J_0\left(\frac{\pi\alpha_{0n''}}{c} r\right) \end{matrix} \right\}, \begin{cases} l_B \le z \le l_B + l_C \\ 0 \le r \le c \end{cases} \end{cases} \tag{2}$$

Moreover, the speed of the acoustic volume is

$$Q(r,z,\omega) = \frac{-S}{i\omega\rho_0}\frac{dp}{dz} \tag{3}$$

From Figure 1, the boundary conditions $\Gamma_1$ and $\Gamma_2$ are the contraction duct discontinuities, whereas $\Gamma_3$ and $\Gamma_4$ are the expansion duct discontinuities. $\Gamma_5$ must meet the boundary conditions $\partial p/\partial n = 0$ and be continuous at the discontinuity $z = 0$ and $z = l_B$.

Lighthill [13] has studied acoustic propagation on sudden changes in the cylinder's cross-section. The propagated wave undergoes reflection and is transmitted only by the plane wave's impedance mismatch, $\rho_0 c_S/S$, with $\rho_0$, $c_S$, and $S$ being the density of the medium, the speed of sound, and the cross-section, respectively.

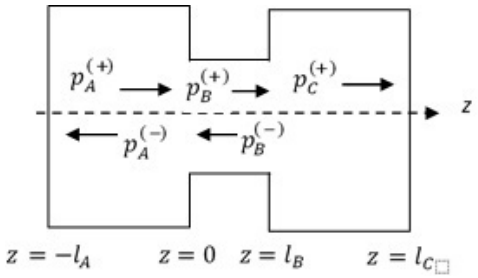


**Figure 2.** H-type microcells acoustic pressure propagation analysis.

Impedance is a fundamental concept in acoustics [13], [14]. On an actual surface or solid object, the impedance is determined by the relationship between the acoustic pressure $p(z,\omega)$ and the normal component of the particle's velocity, $v(z,\omega)$. This relationship depends on the angular frequency, $\omega$.

Impedance can be used as a boundary condition on the surface of a body, and it is possible to solve the problem of waves outside the body without explicitly addressing the inside of it [15], [16], [17] and given by

$$Z(z,\omega) = \frac{p(z,\omega)}{Q(z,\omega)} \tag{4}$$

The problem can be extended if two or more cylinders are connected through parallel axes with different lengths and cross-sectional areas so that the impedance and frequency obtained are highly dependent on the parameters of each cylinder. The geometrical problem of the microcells is critical, especially when duct discontinuity is the main problem in this study, both for contraction and expansion.

### 2.1. Impedance on the H-type Microcells

In acoustics, impedance is a crucial notion [13], [14]. The relationship between the acoustic pressure, $p(z,\omega)$, and the normal component of the particle velocity, $Q(z,\omega)$, at a real surface or solid object determines the impedance. The frequency, $\omega$, affects this relationship. When applied to a body's surface, impedance can be utilized as a boundary condition, making it possible to handle the issue of waves outside the body without specifically addressing its inside [14], [15], [16], [17], [18], [19], [20]).

$$Z(z,\omega) = \frac{p(z,\omega)}{Q(z,\omega)}$$

The issue can be made more complex if two or more cylinders are connected by parallel axes of varying lengths and cross-sectional areas, resulting in an impedance and frequency strongly dependent on each cylinder's characteristics. When the sudden change in cross-sectional area (duct discontinuity) is the main issue in this study, for both acoustic propagation from a large to small cross-sectional cylinder area (contraction) or vice versa (expansion), the geometrical problem of the microcells is a very significant issue.

#### a. Contraction discontinuity

In the propagation of the contraction duct with the boundary conditions $z = -l_A$ and $z = 0$, the impedance is obtained (see Figure 2) Kuttruff [15] as follows :

$$Z_A(0^-) = Z_{0A}\frac{[iZ_{0A}\tan(k_{zA}l_A) - Z_A(-l_A)]}{[iZ_A(-l_A)\tan(k_{zA}l_A) - Z_{0A}]} \tag{5}$$

where

$$Z_{0A} = \frac{\omega\rho_0}{S_A k_{zA}}.$$

If cylinder $A$ is closed at $z = -l_A$ then $Z_A(-l_A) \to \infty$, such that we get

$$Z_A(0^-) = \frac{iZ_{0A}}{\tan(k_{zA}l_A)} \tag{6}$$

In the same way for cylinder $B$ at $z = 0$ and $z = l_B$, we get

$$Z_B(0^+) = Z_{0B}\frac{[Z_B(l_B^-) + iZ_{0B}\tan(k_{zB}l_B)]}{[Z_{0B} + iZ_B(l_B^-)\tan(k_{zB}l_B)]} \tag{7}$$

where

$$Z_{0B} = \frac{\omega\rho_0}{S_B k_{zB}}$$

Cylinders $A$ and $B$ are connected axis-symmetric at $x = 0$. Not all of the incoming waves are transmitted; some are reflected. The first condition that must be met is that on both sides of the discontinuity, the pressure is the same, $p_A = p_B$. Furthermore, the continuity principle requires that the volume velocity at the duct discontinuity must be the same between the left and right sides, $Q(0^-) = Q(0^+)$, that is, the impedance $Z^{(-)} = p_A/v_A$ and $Z^{(+)} = p_B/v_B$ on both sides of the discontinuity are connected by the equation:

$$\frac{Z_A(0^-)}{S_A} = \frac{Z_B(0^+)}{S_B} \tag{8}$$

So that the impedance of the contraction discontinuity is obtained, viz.:

$$Z_B(l_B^-) = iZ_{0B}\frac{[S_B S_B k_{zB} - S_A k_{zA} S_A \tan(k_{zA}l_A)\tan(k_{zB}l_B)]}{[S_A S_A k_{zA}\tan(k_{zA}l_A) + S_B S_B k_{zB}\tan(k_{zB}l_B)]}$$

On the contraction discontinuity, $S_A > S_B$, then the form $S_B k_{zB} S_B \tan(k_{zB}l_B)$ in the denominator of the equation above can be neglected. If we assume that the wavelength of the propagated sound is very small compared to the length of the cylinder, $k_{zA}l_A \ll 1$ and $k_{zB}l_B \ll 1$, then the impedance can be simplified as:

$$Z_B(l_B^-) = iZ_{0B}\frac{S_B^2 k_{zB} - S_A^2 k_{zA}^2 k_{zB} l_A l_B}{S_A^2 k_{zA}^2 l_A} \tag{9}$$

which is a direct consequence of the continuity equation. This proves that any sudden change in the

cross section of the duct acts as an impedance transformer.

### b. Expansion discontinuity

As in cylinder $A$, if cylinder $C$ is closed at $z = l_B + l_C$, then $Z(l_B + l_C) \to \infty$ and because of the discontinuity of the ducts of cylinders $B$ and $C$, $S_B < S_C$ is a form of expansion, and assuming that $k_{zC} l_C \ll 1$ then the equation for the impedance of cylinders $B$ and $C$ becomes:

$$Z_C(l_B^+) = \frac{-iZ_{0C}}{k_{zC} l_C}. \tag{10}$$

If the discontinuity of $AB$ duct is connected to cylinder $C$ and has a discontinuity at $z = l_B$, then:

$$\frac{Z_B(l_B^-)}{S_B} = \frac{Z_C(l_B^+)}{S_C}. \tag{11}$$

By substituting equations (9) and (10) into equation (11) and assuming the dimensions of cylinders $A$ and $C$ are the same, then the longitudinal wave number is obtained as follows:

$$k_{zC}^2 = k_{zA}^2 = \frac{S_B^2}{l_A l_B S_A^2} \tag{12}$$

and the wave number in cylinder $B$ (resonator) has been known previously [21], that is:

$$k_{zB}^2 = \left(\frac{\pi k}{l_B}\right)^2 = k_0^2 - \left(\frac{\pi \alpha_{mn}}{b}\right)^2. \tag{13}$$

Thus, the resonant frequency of the H-type microcell can be obtained by the sum of wave numbers of each cylinder, and assuming $S_A = S_C$, [22]

$$k_0^2 = k_{zA}^2 + k_{zB}^2 + k_{zC}^2$$

that is

$$\omega_{k00} = c_S \sqrt{\frac{4S_B^2}{l_A l_B S_A^2} + \left(\frac{\pi k}{l_B}\right)^2} \tag{14}$$

where $k$, $m$, and $n$ are the longitudinal, azimuthal, and radial normal modes, respectively; $c_s$, $b$, $S_A$, $S_B$, $l_A$, $l_B$, and $\alpha_{mn}$ are the speed of sound in the medium, the radius of cylinders $B$, the cross-sectional areas of cylinders $A$ and $B$, the lengths of cylinders $A$ and $B$, and the $n^{\text{th}}$ root of the equation involving the $m^{\text{th}}$ order Bessel function, respectively.

The wave number in equation (12) is a combination of the dimensions of cylinder $A$ (buffer) and cylinder $B$ (resonator) which shows that the impedance at the duct discontinuity of the microcells is vanishes at a certain resonant frequency, which is the correction factor for the single cylinder resonant frequency, in equation (13).

### 2.2 Transmission Matrix Method (TMM) and Transmission Loss (TL)

The Transmission Matrix Method (TMM), whose foundation is the acoustic behavior of plane waves on a uniform duct element with a length $L$ and uniform fluid flow (average density $\rho_0$ and sound speed $c_S$), Starting with the acoustic wave traveling from the left end at $z = -l_A$ to the right end at $z = l_B + l_C$ through discontinuities at $z = 0$ and $z = l_B$, the H-type microcell system was analyzed in stages [23], [24]. Pressure $p$ and volume velocity $Q$ are what cause this cylinder's propagation. Figure 2 shows the cylinder's acoustic transmission from (1) to (2),

$$\begin{pmatrix} p(-l_A) \\ Q(-l_A) \end{pmatrix} = \begin{pmatrix} A_{11} & A_{12} \\ A_{21} & A_{22} \end{pmatrix} \begin{pmatrix} p(0^-) \\ Q(0^-) \end{pmatrix} \tag{15a}$$

where

$$A_{11} = [\cos(k_{zA} l_A)]$$
$$A_{12} = \left[ i \left(\frac{\rho_0 c_0}{S_A}\right) \sin(k_{zA} l_A) \right]$$
$$A_{21} = \left[ i \left(\frac{S_A}{\rho_0 c_0}\right) \sin(k_{zA} l_A) \right]$$
$$A_{22} = [\cos(k_{zA} l_A)]$$

In the same way, the acoustic propagation analysis can be written in the form of a transmission matrix (3) to (4) and from (5) to (6),

$$\begin{pmatrix} p(0^+) \\ Q(0^+) \end{pmatrix} = \begin{pmatrix} B_{11} & B_{12} \\ B_{21} & B_{22} \end{pmatrix} \begin{pmatrix} p(l_B^-) \\ Q(l_B^-) \end{pmatrix} \tag{15b}$$

where

$$B_{11} = [\cos(k_{zB} l_B)]$$
$$B_{12} = \left[ i \left(\frac{\rho_0 c_0}{S_B}\right) \sin(k_{zB} l_B) \right]$$
$$B_{21} = \left[ i \left(\frac{S_B}{\rho_0 c_0}\right) \sin(k_{zB} l_B) \right]$$
$$B_{22} = [\cos(k_{zB} l_B)]$$

and

$$\begin{pmatrix} p(l_B^+) \\ Q(l_B^+) \end{pmatrix} = \begin{pmatrix} C_{11} & C_{12} \\ C_{21} & C_{22} \end{pmatrix} \begin{pmatrix} p(l_B + l_C) \\ Q(l_B + l_C) \end{pmatrix} \tag{15c}$$

where

$$C_{11} = [\cos(k_{zC} l_C)]$$
$$C_{12} = \left[ i \left(\frac{\rho_0 c_0}{S_C}\right) \sin(k_{zC} l_C) \right]$$
$$C_{21} = \left[ i \left(\frac{S_C}{\rho_0 c_0}\right) \sin(k_{zC} l_C) \right]$$
$$C_{22} = [\cos(k_{zC} l_C)]$$

The Bernoulli equation can be used to determine the transfer matrix for duct discontinuities at $z = 0$, see figure 2. This equation is applied while taking into account the streamline motion equations. Bernoulli's equation asserts that the total head in a fluid system is the same all throughout the system, assuming that there is no shear stress along the streamline. The heads of elevation, pressure, and velocity all make up

the total head. Shear strains can be found both inside a fluid and along the fluid/system boundary in actual systems. Since the total head in a fluid system is not constant as a result, the energy equation accurately captures this fact. The Bernoulli equation and the energy equation have a lot in common. According to the law of continuity, it can be assumed that the energy equation applies to the propagation of pressure and volume velocity. [25]

$$p_{sA}^{(2)} + \frac{1}{2}\rho\left(v_A^{(2)}\right)^2 + \rho g z_A^{(2)} = p_{sB}^{(3)} + \frac{1}{2}\rho\left(v_B^{(3)}\right)^2 + \rho g z_B^{(3)} + \rho g h_e \quad (16)$$

where $p_s$ is the static pressure of the fluid, $\rho$ is the density of the fluid, $z$ is the height of the duct, $g$ is the acceleration due to gravity, and $h_e$ is the head loss. Head loss is potential energy, which is converted into kinetic energy. Head loss is caused by duct system barriers, for example, on valves, fittings, entrances, or connections / changes in size. Supercript 1 indicates the entry side and supersript 2 indicates the exit side. In most cases, the elevation heat difference is negligible, i.e. $z(0^-) = z(0^+)$. Stagnation pressure is the sum of heat pressure and heat velocity, $p = p_s + \frac{1}{2}\rho v^2$. Equation (16) is reduced to

$$p(0^-) = p(0^+) + \rho g h_e \quad (17)$$

Equation (15) can also be written as a function of the heat loss coefficient, $k_e$

$$p(0^-) = p(0^+) + \frac{1}{2}k_e\rho\left(v(0^+)\right)^2 \quad (18)$$

The term pressure loss in equation (17) or (18) is usually a function of the volume of fluid flowing through the system $Q$. So equation (17) can be written

$$p(0^-) = p(0^+) + R_f Q(0^+) \quad (19)$$

where $R_f$ is the flow resistance. On the other hand, the sum of the flows entering the system is equal to the amount leaving the system

$$Q(0^-) = Q(0^+) \quad (20)$$

By comparing equations (8) and (10), the flow resistance related to head loss is

$$R_f(Q) = \frac{\rho g h_e(Q)}{Q} \quad (21)$$

20which is the head loss, and as a result the flow resistance, depends on the flow. By comparing equations (18) and (19) the flow resistance is associated with a loss coefficient of

$$R_f(Q) = k_e \frac{\rho}{2S^2}|Q| \quad (22)$$

where $S$ is the cross-sectional area of the inlet or outlet. The loss coefficient is a constant that depends on the duct geometry.

The problem of duct discontinuity in the form of expansion and contraction is treated separately. For the case of expansion, consider steady flow in the duct with sudden enlargement. The energy equation (17) can be written ignoring the potential energy difference

$$R_f Q = p(0^-) - p(0^+) + \rho\frac{\left(v(0^-)\right)^2 - \left(v(0^+)\right)^2}{2} \quad (23)$$

Applying Newton's second law, the net force acting on the fluid is equal to the rate of increase in momentum

$$\left(p(0^-) - p(0^+)\right)S_B = \rho Q\left(v(0^+) - v(0^-)\right) \quad (24)$$

Substituting equation (24) into (23) gives

$$R_f = \rho\frac{v(0^+)\left(v(0^+) - v(0^-)\right)}{Q} + \rho\frac{\left(v(0^-)\right)^2 - \left(v(0^+)\right)^2}{2Q} \quad (25)$$

which is reduced to

$$R_{f\to \mathrm{e}} = k_{e\to e}\frac{\rho}{2S_A^2} \quad (26)$$

where $k_{e\to e}$ is the coefficient of expansion loss and is equal to equation (17)

$$k_{e\to \mathrm{e}} = \left(1 - \frac{S_B}{S_C}\right)^2 \quad (27)$$

For the case of contraction, the loss coefficient for sudden contraction depends on the area ratio and is given by equations (21) and (18)

$$R_{f\to c} = k_{e\to c}\frac{\rho}{2S_B^2} \quad (28)$$

where $k_{e\to c}$ is the contraction loss coefficient [25]

$$k_{e\to c} = \left(1 - \frac{S_B}{S_A}\right)^2 \quad (29)$$

From the explanation, it can be written

$$\left.\begin{matrix} p(0^-) = p(0^+) + R_c Q(0^+) \\ p(l_B^-) = p(l_B^+) + R_e Q(l_B^+) \end{matrix}\right\} \quad 0 < r < b$$

$$\left.\begin{matrix} Q(0^-) = Q(0^+) \\ Q(l_B^-) = Q(l_B^+) \end{matrix}\right\} \quad 0 < r < b \qquad (30)$$

$$Q(0^+) = 0, \quad b < r < a$$

$$Q(l_B^-) = 0, \quad b < r < c$$

So the form of transfer matrix at the discontinuity of cylinder $A$ and $B$ (contraction)

$$\begin{pmatrix} p(0^-) \\ Q(0^-) \end{pmatrix} = \begin{pmatrix} 1 & R_c \\ 0 & 1 \end{pmatrix} \begin{pmatrix} p(0^+) \\ Q(0^+) \end{pmatrix} \qquad (31)$$

and on cylinder $B$ and $C$ (expansion)

$$\begin{pmatrix} p(l_B^-) \\ Q(l_B^-) \end{pmatrix} = \begin{pmatrix} 1 & R_e \\ 0 & 1 \end{pmatrix} \begin{pmatrix} p(l_B^+) \\ Q(l_B^+) \end{pmatrix} \qquad (32)$$

The transmission from $(-l_A)$ to $(l_B + l_C)$ from equation (15a), (15b), (15c), (31) and (32) is obtained,

$$\begin{pmatrix} p(-l_A) \\ Q(-l_A) \end{pmatrix} = \begin{pmatrix} T_{11} & T_{12} \\ T_{21} & T_{22} \end{pmatrix} \begin{pmatrix} p(l_B + l_C) \\ Q(l_B + l_C) \end{pmatrix} \qquad (33)$$

where

$$\begin{pmatrix} T_{11} & T_{12} \\ T_{21} & T_{22} \end{pmatrix} = \begin{pmatrix} A_{11} & A_{12} \\ A_{21} & A_{22} \end{pmatrix} \begin{pmatrix} 1 & R_c \\ 0 & 1 \end{pmatrix} \begin{pmatrix} B_{11} & B_{12} \\ B_{21} & B_{22} \end{pmatrix} \begin{pmatrix} 1 & R_e \\ 0 & 1 \end{pmatrix} \begin{pmatrix} C_{11} & C_{12} \\ C_{21} & C_{22} \end{pmatrix}$$

There are at least three crucial considerations to make while using this method. Noise reduction (NR), insertion loss (IL), and transmission loss (TL) are the first three. It is employed in this situation since TL does not rely on the sound source and because it takes latitude variations into account while calculating propagation effects. As long as sonic propagation occurs, it is assumed that the pressure and volume velocity in the duct and in the duct discontinuity from the source intake to the outlet remain unaltered. The majority of sound calculations are based on the relationship between the sound's frequency (measured in Hz), and sound's intensity (measured in dB). Sound can be affected by a number of environmental conditions, such as pressure, temperature, and medium density [15].

$$TL(l_A, l_B, l_C, S_A, S_B, S_C) = 10 \log\left(\frac{|T_{11} + T_{12} + T_{21} + T_{22}|}{2}\right) + 10 \log\left(\frac{S_A}{S_C}\right) \qquad (34)$$

## 3. GENETIC ALGORITHMS (GAs)

The concept of GAs–was first formalized by Holland (1975) and extended to functional optimization by Jong (1975). Later on, the GAs involved the use of optimization search strategies pattern after the Darwinian notion of natural selection and evolution Haupt and Haupt [26]. The GA accomplishes the task of optimization by starting with a random “population" of values for the parameters of an optimization problem. Thereafter, a new “generation" with improved objective function values is produced. The binary system is used to achieve evolution in the latest generation. The binary system is a representation of real numbers and integers. In addition, by manipulating the strings, the operators of reproduction, crossover, mutation, and elitism are thus at work sequentially. A brief description of GA operators and their components is as follows [27], [28], [29], [30], [31]:

a. Populations and Chromosomes: The initial population begins by randomization. The parameter set is encoded to form a string representing the chromosome. By evaluation of the objective function, each chromosome is assigned fitness.
b. Parent: Using the probabilistic computation weighted by relative fitness, pairs of chromosomes are selected as parents. Each individual in the population is assigned a space on the roulette wheel proportional to their relative fitness. Individuals with the largest portion on the wheel have the most significant probability of being selected as the parent generation for the next generation.
c. Offspring: Crossover generates one pair of offspring from the selected parent. Crossover occurs with a probability of pc. Then, random selection is made from the crossover and combination of the 2 oldest genetic data. The single-point crossover scheme was chosen from the GA optimization. Recombination and parent selection are the principal methods for the evolution of the GA.

d. Mutation: This operator provides the needed diversity in the population and searches different areas. Genetically, a mutation occurs with a probability of pm where the new and unexpected points are brought into the GA optimizer's search domain. This essential operator introduces diversity into the population and prevents the GA from becoming saturated with solutions at the local optimum.
e. Elitism: Elitism reintroduces the best candidate in each generation. It can prevent the best gene from disappearing and improves optimization accuracy during reproduction.
f. New Generation: Reproduction includes selection, crossover, mutation, and elitism. The reduplication continues until a new generation is constructed and the original generation is substituted. Highly fit characteristics produce more copies of themselves in subsequent generations, resulting in a movement of the population toward an optimal direction. The process can be terminated when the number of predetermined maximum generations (gen_no) has been reached.

The GA method starts by generating random numbers from 0 to 1 in a matrix, which is then converted into binary numbers 0 and 1 (by rounding to 0 if < 0.5 and 1 if > 0.5). This stored binary number is called population initiation. The next step is the evolution process, which starts with decoding the chromosomes into a fitness function that produces a fitness value. This fitness value is processed to get the desired output variable values. Next, the code is converted back to the binary chromosome called encoding. The next step is to sort each individual in the population according to their fitness.

The evaluation process is the primary process in this optimization. This process is a bridge between the physical phenomena and the program created. After the evaluation process, the binary chromosomes from the encoding results are matched to reach optimization (threshold). If not achieved, then the next step is the reproduction process. Reproduction is the most essential part of the biological process to get a better generation. The first step is copying the best chromosomes from each population, which is elitism. Next is selecting parents using a roulette wheel selection, in which the two selected parents will be mated. The mating is carried out by crossing one intersection point, producing two offspring. The reproduction process will still be ongoing, and some genes in the offspring's chromosomes will undergo mutations.

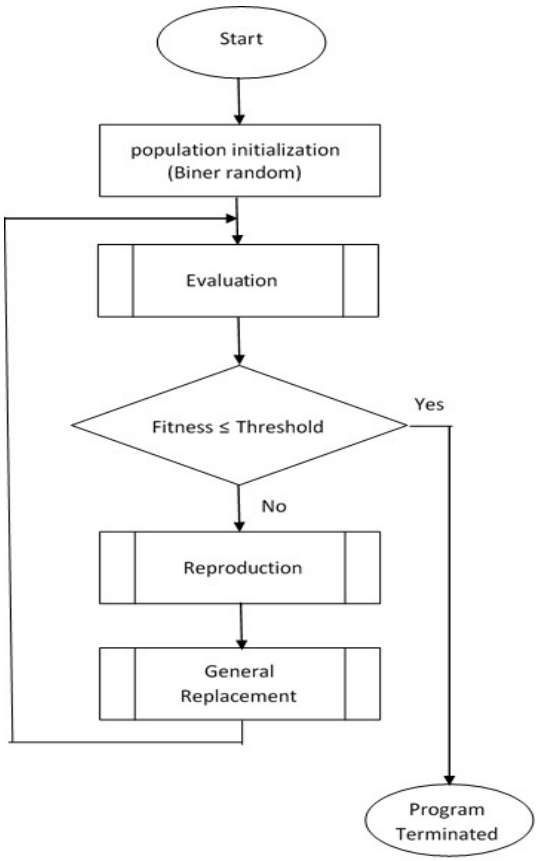


**Figure 3.** Main Program of GA

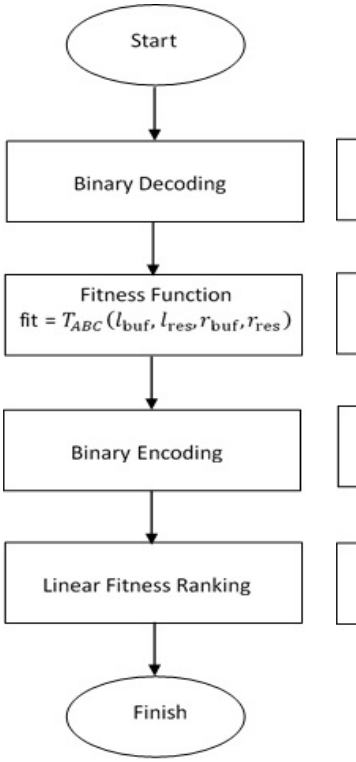


**Figure 4.** Sub-program of Evaluation

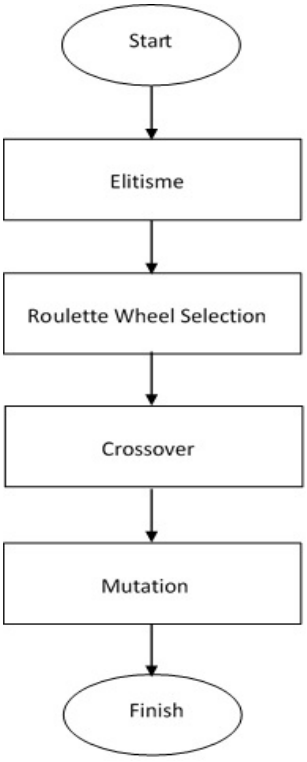


**Figure 5.** Sub-program of Reproduction

The following process completely replaces the old with the new generation. The latest generation from the general replacement results is re-evaluated until

the process is stopped if optimization is achieved or until the last generation is processed. The flowchart of the GA for the analysis of the H-type microcell optimization is given in Figure 3.

**Results and Discussion**

According to Bijnen [32], this H-type microcell has the following dimensions: buffer length ($l_{\mathrm{buf}}$) = 50 mm, resonator length ($l_{\mathrm{res}}$) = 100 mm, buffer radius ($r_{\mathrm{buf}}$) = 9 mm, and resonator radius ($r_{\mathrm{res}}$) = 3 mm. The fluid utilized is ethylene gas ($C_2H_4$).

The length of the buffer ($l_{\mathrm{buf}}$) and resonator ($l_{\mathrm{res}}$), as well as the radius of the buffer ($r_{\mathrm{buf}}$) and resonator ($r_{\mathrm{res}}$), are the study's optimization parameters. The initial population (pop), crossover probability (pc), mutation probability (pm), maximum generation (itermax), and tolerance value (toll) are additional parameters utilized in this genetic method. These parameters have values of 30, 0.95, 0.005, 100, and $10^{-20}$, respectively. The gases used are ethylene ($C_2H_4$) and oxygen ($O_2$). Physical parameters of ethylene gas used are density 1.178 $\mathrm{kg/m^3}$, heat capacity ratio 1.24, molar mass 0.02805 kg/mol, viscosity $1.028 \times 10^{-5}$ Pa.s, thermal conductivity $20.362 \times 10^{-3}$ W/(m.K), and specific heat at constant pressure 42.9 J/(mol.K), while oxygen gas used are density, heat capacity ratio, molar mass, viscosity, thermal conductivity, and specific heat at constant pressure with respective values of 1.284 $\mathrm{kg/m^3}$, 1.395, 0.032 kg/mol, $2.04 \times 10^{-5}$ Pa.s, $26.58 \times 10^{-3}$ W/(m.K), and 29.378 J/(mol.K).

**Table 1.** Optimization results of GA on microcell for longitudinal modes $[klm] = [100]$ for ethylene gas.

| $l_{\mathrm{buff}}$ (mm) | $l_{\mathrm{res}}$ (mm) | $r_{\mathrm{buff}}$ (mm) | $r_{\mathrm{res}}$ (mm) | frequency (Hz) | TL (dB) |
|---|---|---|---|---|---|
| 48.75 | 107.47 | 8.79 | 2.93 | 1543.73 | 102.40 |
| 48.75 | 107.46 | 8.78 | 2.93 | 1543.86 | 103.10 |
| 48.75 | 107.47 | 8.78 | 2.93 | 1543.79 | 102.40 |
| 48.82 | 107.47 | 8.78 | 2.93 | 1543.78 | 102.40 |
| 48.76 | 107.47 | 8.78 | 2.93 | 1543.79 | 102.40 |

**Table 2.** Optimization results of GA on microcell for longitudinal modes $[klm] = [100]$ for oxygen gas.

| $l_{\mathrm{buff}}$ (mm) | $l_{\mathrm{res}}$ (mm) | $r_{\mathrm{buff}}$ (mm) | $r_{\mathrm{res}}$ (mm) | frequency (Hz) | TL (dB) |
|---|---|---|---|---|---|
| 48.78 | 107.47 | 8.78 | 2.93 | 1543.76 | 102.80 |
| 48.75 | 107.46 | 8.78 | 2.93 | 1543.93 | 103.10 |
| 48.75 | 107.47 | 8.79 | 2.93 | 1543.74 | 102.70 |
| 48.83 | 107.47 | 8.78 | 2.93 | 1543.78 | 102.80 |
| 48.75 | 107.47 | 8.78 | 2.93 | 1543.79 | 102.80 |

Transmission loss (TL) and resonant frequency ($f$) have a close relationship influenced by the wave propagation pattern. The wave pressure, which depends on the dimensions of the H-type microcell, changes in response to a sudden change in the cross-sectional area of the duct; hence, a duct with a large cross-sectional area has a slight pressure, and vice versa (head loss). The wave must consider "edge conditions" when it encounters the duct wall at the discontinuity, which mandates that the energy of the surrounding total field be constrained. As a result, a unique solution is produced directly tied to optimizing the microcell design, which is crucial to achieving the highest wave pressure.

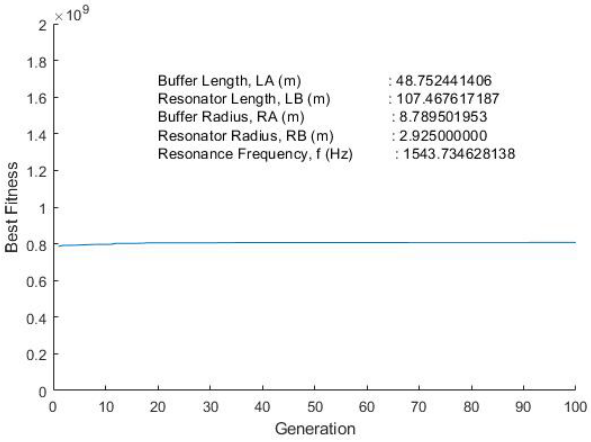


(a) Ethylene Gas

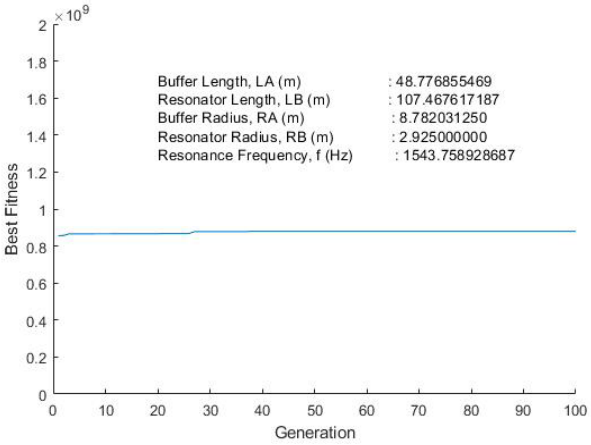


(b) Oxygen Gas

**Figure 6.** Optimal Design and Resonance Frequency

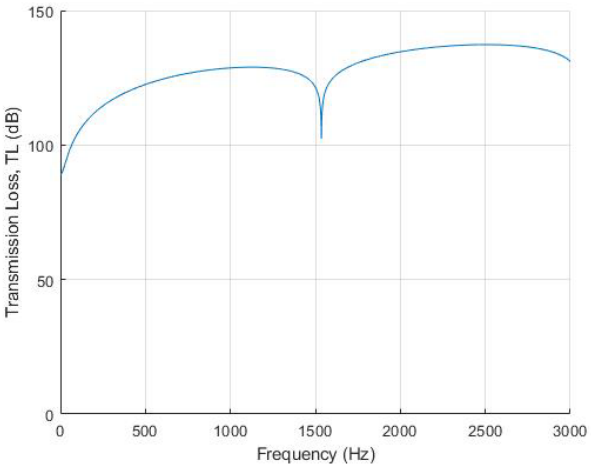


(a) Ethylene Gas

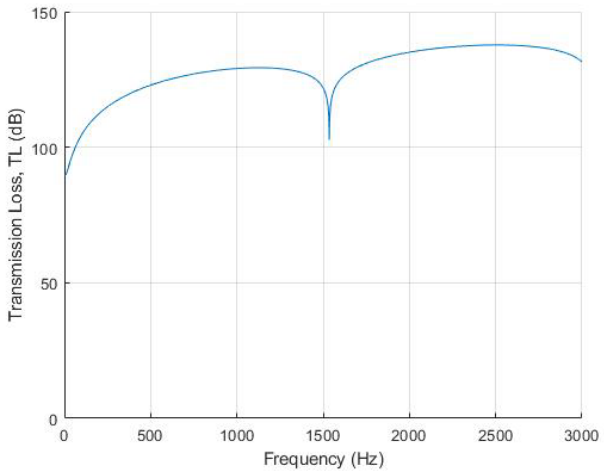

(b) Oxygen Gas

**Figure 7.** Transmission Loss (TL)

## 4. CONCLUSION

The configuration of the physical parameter values for these H-type microcells has values that are similar to one another. This means that the resonant frequency is also within that range. The TL in the microcells is related to the strength of the incoming wave, which will experience transmission losses when passing through the microcell's discontinuity

Tables 1 and 2 of ethylene and oxygen gas show that the buffer and resonator sizes have very small differences, both almost always having the same resonant frequency and TL. Transmission losses are greatly influenced by the design of the buffer and resonator dimensions, so the smallest TL value is expected. In this study, the smallest TL value in the range of 102.4 dB - 103.1 dB was achieved with a buffer length in the range of 48.75 mm - 48.83 mm, a buffer radius in the range of 8.78 mm - 8.79 mm, a microcell length of range 107.46 mm - 107.47 mm, and microcell radius 2.93 mm, with a resonance frequency in the range 1543.73 Hz - 1543.93 Hz.

The collision and fluid friction with the channel walls will cause head loss, which results in changes in acoustic pressure when passing through channel discontinuities, which cannot be ignored. By using the transmission matrix method (TMM) and genetic algorithm (GA) to analyze acoustic propagation in H-type microcells, configure the physical parameter values, namely the length ($l_{\mathrm{buf}}$) and radius ($r_{\mathrm{buf}}$) of the buffer, length ($l_{\mathrm{res}}$) and radius ($r_{\mathrm{res}}$) micro cells, and the values of transmission loss (TL) and resonant frequency ($f$) are obtained.

The design of type H cylindrical microcells was optimized by considering the impedance limit requirements. The geometric shape of H-type microcells undergoes sudden contraction and expansion, dramatically affecting their transmission coefficient. The TL value must be as small as possible to obtain a large acoustic transmission coefficient, and the GA method provides optimal buffer and microcell sizes.

## ACKNOWLEDGMENT

We would like to express our thanks because this research was fully supported by Yogyakarta State University (UNY) Research Group funds in 2023 with contract number B/44/UN34.13/PT.01.03/2023

## REFERENCES

[1] J. W. Miles, "The Analysis of Plane Discontinuities in Cylindrical Tubes. Part II," *J Acoust Soc Am*, vol. 17, no. 3, pp. 271–284, 1946.

[2] J. W. Miles, "The Analysis of Plane Discontinuities in Cylindrical Tubes. Part I," *The Journal of the acousticsal society of america*, vol. 17, no. 3, pp. 259–271, 1946.

[3] F. C. Karal, "The Analogous Acoustical Impedance for Discontinuities and Constrictions of Circular Cross Section," *J Acoust Soc Am*, vol. 25, no. 2, pp. 233–237, 1953.

[4] M. Tavakoli, A. Tavakoli, M. Taheri, and H. Saghafifar, "Design, simulation and structural optimization of a longitudinal acoustic resonator for trace gas detection using laser photoacoustic spectroscopy (LPAS)," *Opt Laser Technol*, vol. 42, no. 5, pp. 828–838, 2010, doi: 10.1016/j.optlastec.2009.12.012.

[5] Y. Cai, N. Arsad, M. Li, and Y. Wang, "Buffer structure optimization of the photoacoustic cell for trace gas detection," *Optoelectron Lett*, vol. 9, no. 3, pp. 233–237, May 2013, doi: 10.1007/s11801-013-3017-3.

[6] L. Duggen, N. Lopes, M. Willatzen, and H. G. Rubahn, "Finite element simulation of photoacoustic pressure in a resonant photoacoustic cell using lossy boundary conditions," *Int J Thermophys*, vol. 32, no. 4, pp. 774–785, 2011, doi: 10.1007/s10765-010-0828-3.

[7] J. M. Rey, D. Marinov, D. E. Vogler, and M. W. Sigrist, "Investigation and optimisation of a multipass resonant photoacoustic cell at high absorption levels," *Appl Phys B*, vol. 80, no. 2, pp. 261–266, Feb. 2005, doi: 10.1007/s00340-004-1705-1.

[8] J. M. Rey and M. W. Sigrist, "Differential mode excitation photoacoustic spectroscopy : A new photoacoustic detection scheme Differential mode excitation photoacoustic spectroscopy : A new photoacoustic detection scheme," vol. 063104, no. 2007, 2012, doi: 10.1063/1.2746817.

[9] M. Mannoor, J. Hwang, and S. Kang, "Numerical study of geometrical effects on the performance of an H-type cylindrical resonant photoacoustic cell," *Journal of Mechanical Science and Technology*, vol. 32, no. 12, pp. 5671–5683, 2018, doi: 10.1007/s12206-018-1114-8.

[10] K. S. Peat, "The acoustical impedance at discontinuities of ducts in the presence of a mean flow," *J Sound Vib*, vol. 127, no. 1, pp. 123–132, 1988, doi: 10.1016/0022-460X(88)90353-7.

[11] R. Y. A. Sari, A. Bambang, Mitrayana, and D. Lelono, "Pengaruh Konfigurasi Geometri Buffer Resonator Tipe-H Terhadap Intensitas Bunyi," *Jurnal Sains Dasar*, vol. 9, no. 1, pp. 30–36, 2020.

[12] B. Liu, J. Liu, W. Wei, H. Shen, and Z. Wei, "Suppression of low frequency sound transmission in fluid-filled pipe systems through installation of an anechoic node array," *AIP Adv*, vol. 8, no. 11, 2018, doi: 10.1063/1.5051603.
[13] L. E. Kinsler, A. R. Frey, A. B. Coppens, and J. V. Sanders, *Fundamentals of Acoustics*, 4 th. 2000.
[14] D. Noreland, "Impedance boundary conditions for acoustic waves in a duct with a step discontinuity," *Comput Methods Appl Mech Eng*, vol. 71, no. 2, pp. 197–224, 2003.
[15] H. Kuttruff, *Acoustic An Introduction*. Taylor & Francis, 2006.
[16] A. Chaigne and J. Kergomard, *Acoustics of Musical Instruments*. Springer Verlag New York, 2016.
[17] Y. H. Kim, *Sound Propagation: An Impedance Based Approach*. 2010. doi: 10.1016/B978-0-12-811240-3.00002-3.
[18] R. Y. A. Sari, A. B. S. Utomo, Mitrayana, and D. Lelono, "Impedance Boundary Conditions on The Optimal Design of the H-Type Cylinder Resonator Using Transmission Matrix Method and Genetic Algorithm," *Romanian Journal of Acoustics and Vibration*, vol. 19, no. 1, pp. 3–12, 2022.
[19] R. Y. Sari, A. B. S. Utomo, Mitrayana, D. Lelono, and Supardi, "SINGULARITAS EFEK TEPI DARI DISKONTINUITAS SALURAN PADA RESONATOR SILINDER TIPE-H," *Jurnal. Sains Dasar*, vol. 2022, no. 1, pp. 46–57, 2022.
[20] R. Y. A. Sari, A. B. S. Utomo, Mitrayana, and D. Lelono, "Pengaruh konfigurasi geometri buffer terhadap intensitas bunyi dari perambatan akustik pada resonator tipe-H," *Jurnal Sains Dasar*, 2020.
[21] J. P. Besson and L. Thévenaz, "Photoacoustic spectroscopy for multi-gas sensing using near infrared lasers," *Laboratoire de nanophotonique et métrologie*, vol. Ph.D., no. Thèse No. 3670 (2006), pp. 1–189, 2006, doi: 10.5075/epfl-thesis-3670.
[22] M. Bruneau, Ch. Garing, and H. Leblond, "Quality factor and boundary-layer of lower order modes in acoustic cavities," *J. Physique 46*, vol. 46, pp. 1079–1085, 1985.
[23] F. Chen, "Optimization design of muffler based on acoustic transfer matrix and genetic algorithm," *Journal of Vibroengineering*, vol. 16, no. 5, pp. 2216–2223, 2014.
[24] M. Ranjbar, H. Arslan, and M. Orak, "Effect of Geometry Modification on Sound Transmission Loss in Multi-Chamber Muffler," in *The 8th International Conference on Acoustics & Vibration (ISAV2018)*, 2018, pp. 1–12.
[25] T. Elnady, S. Elsaadany, and M. Åbom, "Flow and pressure drop calculation using two-ports," *Journal of Vibration and Acoustics, Transactions of the ASME*, vol. 133, no. 4, pp. 1–8, 2011, doi: 10.1115/1.4003593.
[26] R. L. Haupt and S. E. Haupt, *Practical genetic algorithms*. 2004. doi: 10.1007/11543138_2.
[27] A. J. Chipperfield and P. J. Fleming, "MATLAB Genetic algorithm toolbox," *IEE Colloquium (Digest)*, no. 14, 1995.
[28] J. McCall, "Genetic algorithms for modelling and optimisation," *J Comput Appl Math*, vol. 184, no. 1, pp. 205–222, 2005, doi: 10.1016/j.cam.2004.07.034.
[29] L. J. Yeh, Y. C. Chang, and M. C. Chiu, "Shape optimal design on double-chamber mufflers using simulated annealing and a genetic algorithm," *Turkish Journal of Engineering and Environmental Sciences*, vol. 29, no. 4, pp. 207–224, 2005, doi: 10.3906/sag-1206-82.
[30] N. Bramantyo, "Desain Resonator Hemlholtz Ganda dengan Menggunakan Matlab," Universitas Sebelas Maret, 2006.
[31] S. Samanta, "Genetic Algorithm : An Approach for Optimization ( Using MATLAB )," *Int J Latest Trends Eng Technol*, vol. 3, no. 3, pp. 261–267, 2014.
[32] F. G. C. Bijnen, J. Reuss, and F. J. M. Harren, "Geometrical optimization of a longitudinal resonant photoacoustic cell for sensitive and fast trace gas detection," *Review of Scientific Instruments*, vol. 67, no. 8, pp. 2914–2923, 1996, doi: 10.1063/1.1147072.